Thermal Convection in a Rotating Fluid Annulus: Part 1. The Basic Axisymmetric Flow

GARETH P. WILLIAMS

Geophysical Fluid Dynamics Laboratory, ESSA, Washington, D. C.

(Manuscript received 6 September 1966)

ABSTRACT

The thermally driven motion of a fluid contained in a rotating annulus is investigated by numerical integration of the Navier-Stokes equations as an initial value problem. Four distinct regimes of hydrodynamical flow can exist in the annulus system. This paper will consider the nature and computational requirements of the axisymmetric state for its own sake and partly as a prelude to a quantitative study of the more complex irregular regime. Calculations were made for two flows whose parameters, with the exception of the rotation rates, are identical, and whose upper surfaces are free. How the axisymmetric state varies with the Rossby and Taylor parameters will be discussed in Part 2.

The solutions show that the flow forms a direct circulation with countercurrents on both side walls, and with a strong flow from the base of the hot wall, across the interior, up toward the top of the cold wall. The thermal boundary layers form in small and isolated regions near the top of the cold wall and base of the hot wall. The fluid and container effect most of their heat exchange through these discrete regions. The isotherms slope up toward the cold wall and a large region of constant temperature exists near the fluid surface. The higher rotation rate makes the isotherms more vertical and, as a consequence, the Nusselt number is inversely proportional to the first power of the rotation rate. The upper three-fourths of the fluid flows in the same zonal direction as the rotation, while the remainder flows in the opposite direction. Although the fluid interior is essentially geostrophic, the nonlinear terms do make a significant contribution to the vorticity balance. The angular momentum has a single sink region; this occurs at the top of the cold inner cylinder, and the fluid ignores the potential maximum source at the (hot) outer cylinder. The contributions of the sidewall boundary layers to the energy transformation oppose each other; this leaves the interior region of the fluid as a significant source of energy. Application of Eady's criterion for baroclinic instability when applied to the solutions, shows one flow to be stable, the other unstable. This conclusion agrees with observation.

Contours of the transient fields show the predominately isothermal evolution of the flow towards a steady state. The close association of the sidewall countercurrents to the sidewall boundary layers appears at all stages of development.

Changing the number of grid points used and repeating the calculations demonstrated the accuracy of the solutions.

1. Introduction

The rotating annulus experiments described by Fultz *et al.* (1959) and Hide (1958) exhibit many modes of hydrodynamical behavior, ranging from flow patterns in steady state through those that oscillate periodically to others that vary in an apparently irregular manner. In these experiments, two coaxial cylinders containing water rotate about their axis. If the temperatures of the cylinders are held fixed and if the rate of rotation is sufficiently low, a symmetric steady state circulation develops. If the rotation rate is increased, waves develop which travel at a uniform rate without changing their form. Most of the motion is confined to a jet. On further increasing the rotation rate, an irregular wave pattern forms and moves and changes its shape in an irregular aperiodic manner. Intermediate to the steady wave and irregular wave regimes, "vacillation" occurs in which the waves undergo periodic changes in *pattern*.

The flow in the irregular regime is regarded as a possible analogue of the motion of a planetary atmosphere and so the annulus experiments guide such studies as those of baroclinic instability, and atmospheric periodicity and predictability. If this analogue is correct, then a full explanation of the qualitative features of the atmosphere requires quantitative considerations, for the experiments suggest that under different heating and rotation rates the motion of the atmosphere might vary in a periodic manner.

The far-reaching consequences drawn from the annulus experiments make it imperative that these experiments be analyzed as thoroughly as possible. The degree of accuracy behind this analogue concept has lacked quantitative establishment mainly because of the difficulty of observation in both the annulus and atmosphere. However, the continuing acquisition of atmospheric data and the creation of model-atmosphere statistics by numerical integration provide an ever-improving understanding of the present state of the atmosphere and the way it functions. In the annulus, on the other hand, the gathering of data has been mainly for the purpose of examining the effect of various

parameter values and physical characteristics upon the formation of the different regimes, the transition of the fluid from one regime to another, and upon the various wave types. The few examinations of the internal structure of the flow that have been made, have yielded some data for the symmetric flows, but the data in general is limited and no conclusions can be drawn about the mechanisms operating. In spite of this lack of detail about the flow, the experimental results on transition phenomena are sufficiently accurate to provide a basis for the theoretical examination of either the transition phenomena alone, or the transition phenomena and detailed structure. From the theoretical viewpoint an accurate explanation of the transition phenomena indicates a possibly accurate prediction of flow details.

Although theory has been in good qualitative agreement with experimental observation of the transition of the fluid from the symmetric regime to the steady wave regime, the quantitative discrepancy has been large. For most theories the inherent simplifications, such as neglect of boundary layers, imply that the physical system being examined resembles *a priori* the atmospheric system, and as such, these theories cannot be regarded as an explanation of annulus mechanics; in some cases the equations are simplified to the extent that their solutions can be regarded as (approximately) describing either the atmosphere or the laboratory experiments. Attempts by Barcilon (1964) and Lorenz (1962) to make theory more realistic by including the boundary layer on the base in parametric form did not provide the quantitative agreement required. The large quantitative disagreement between theory and observation suggests that the neglected sidewall boundary layers must be playing a definite rôle in the annulus flow and that their inclusion in a theoretical treatment is not only essential for quantitative agreement but that it is also necessary in order to make the model represent a true annulus system.

To understand the annulus system and compare it with the atmosphere, its theory must be quantitatively accurate. For this to be so, the important nonlinear processes such as boundary layer phenomena must be accounted for. As in the atmospheric case, the most detailed and comprehensive treatment of all contributing physical entities can be most easily made by a numerical treatment of the problem. The study of the various modes of fluid behavior in the annulus is in a situation comparable to atmospheric studies in that numerical experiments are essential for progress in both fields.

While numerical solutions of annulus flow should show the similarity to the atmospheric system, the results should also provide the necessary quantitative details for further analytical examinations and give a better understanding of the observed features. Furthermore, the equations describing the annulus flow and their numerical treatment exhibit great similarity to those used in atmospheric studies, and for this reason there is interest in the behavior of these analogous equations and their capability to describe a definitive, accessible, analogous physical system. On the physical side, the flow in a rotating annulus offers the simplest available example of quasi-geostrophic baroclinic flow, and if it can be shown that the sidewall boundary layers do play an essentially passive mechanical rôle, then we have at our disposal an excellent system for studying possible atmospheric mechanical forms in pure, isolated form. Although models are becoming more complex, the most significant advances in meteorology have come from studies which have isolated essential mechanisms.

The flows in the wave regime provide a simple example of a nonlinear wave motion. The nonlinear interaction of modes in the vacillating and irregular wave motions could provide reasons for the existence (or non-existence) of periodicities and transition hysteresis in baroclinic flows. Furthermore, simple relationships could possibly be deduced from the numerical solutions, relationships which cannot be deduced from the differential equations, but which would provide a turbulence theory to describe the mean structure of irregular regime flows. These relationships could provide the needed link in the formulation of such a turbulence theory for the atmosphere.

To commence the evaluation of annulus motions by numerical methods, this paper will present the results of computations made for two flows under the assumption that the flow is symmetric about the axis of rotation. Lorenz's (1962) work indicates that steady symmetric flow is mathematically possible under all combinations of rotation and symmetric heating. Likewise, we have obtained a symmetric solution for a parameter combination under which observations would indicate the existence of a wave regime. The present solution also leads to the conclusion that even under parameter conditions for which a wave motion would be expected, a steady state symmetric circulation exists in the mathematical sense, although such a flow cannot be observed experimentally because of its instability. The main aim of the present paper is to study the symmetric types of flow in their own right and from the numerical point of view to investigate the problems of resolution involved in dealing with boundary layers explicitly. The encouraging outcome of these calculations indicates the practicality of considering the more complex and interesting modes of annulus behavior and these will be the subject of a subsequent paper.

2. Equations of axisymmetric transfer and method of integration

We consider a fluid contained between two coaxial cylinders of inner and outer radii a, b, respectively, and two parallel horizontal planes. Let the container

rotate with respect to an inertial system at a constant rate $\boldsymbol{\Omega}$, where the rotation vector, anti-parallel to gravity $\boldsymbol{g}$, coincides with the axis of the cylinders. Motion is considered relative to the solid rotation, and is measured in cylindrical coordinates r, z based on the axis, r being radial and z vertical, with u, v, w as the velocity components in the zonal, radial and vertical directions. The fluid is thermally driven away from the state of solid rotation by an imposed horizontal temperature gradient ΔT, i.e., the inner and outer cylindrical walls are held at different constant temperatures, T_a and T_b. The base is thermally insulating and the surface (at height $z=d$) behaves in the same way owing to the presence of a lid (not in contact) inhibiting interaction with the overlying air.

The explicit assumptions defining the mathematical model applied to the annulus system are:

a) The kinematic viscosity ν, the thermometric conductivity κ, and the coefficient of thermal expansion β are constant. This assumption is made for convenience only.

b) A linear dependence of density ρ on temperature T alone is taken as the equation of state, $\rho=\rho_0[1-\beta(T-T_a)]$, and the coefficient of thermal expansion is taken to be zero except when coupled with the gravitational constant. With the assumption of local incompressibility, this system forms the Boussinesq approximation.

c) Frictional dissipation is negligible in the energy equation.

d) The centrifugal acceleration is much smaller than the gravitational acceleration, i.e., $\Omega^2(a+b)/2g\ll 1$. As a consequence we take the upper surface as being of constant height at every instant. This is absolutely so with a rigid contact lid but for a non-contact lid it implies the assumption that the free surface behaves in the same way as a free slip rigid contact lid.

e) The flow is symmetric about the axis.

While the above assumptions only slightly modify the physical problem, they do offer convenient mathematical simplification without reducing the essential nature of the Navier-Stokes equations. These equations upon writing the hydrostatic pressure deviation as $\pi=p/\rho$, are:

$$\dot{u}+\left(2\Omega+\frac{u}{r}\right)v=\nu\left[u_{zz}+\left(\frac{1}{r}(ru)_r\right)_r\right], \tag{1}$$

$$\dot{v}-\left(2\Omega+\frac{u}{r}\right)u=-\pi_r+\nu\left[v_{zz}+\left(\frac{1}{r}(rv)_r\right)_r\right], \tag{2}$$

$$\dot{w}=-\pi_z+g\beta(T-T_a)+\nu\left[w_{zz}+\frac{1}{r}(rw_r)_r\right], \tag{3}$$

$$\dot{T}=\kappa\left[T_{zz}+\frac{1}{r}(rT_r)_r\right], \tag{4}$$

$$(rv)_r+(rw)_z=0. \tag{5}$$

In the above $(\dot{})=(\ )_t+v(\ )_r+w(\ )_z$ is the total derivative (the subscripts denote partial derivatives and t the time variable).

It is convenient to eliminate the p, v and w variables by introducing a stream function ψ and vorticity ζ to describe the flow in the vertical r, z plane. These are defined as

$$rv=-\psi_z,\quad rw=\psi_r,\quad \zeta=v_z-w_r \tag{6}$$

and give the basic set of equations with which the computations are performed. With a non-dimensional temperature $\theta\equiv(T-T_a)/(T_b-T_a)$, these are:

$$\zeta_t+J(\zeta/r)=-\beta g\Delta T\theta_r+2u_z\left(\Omega+\frac{u_z}{r}\right)+\nu\left[\zeta_{zz}+\left(\frac{1}{r}(r\zeta)_r\right)_r\right], \tag{7}$$

$$\theta_t+\frac{1}{r}J(\theta)=\kappa\left[\theta_{zz}+\frac{1}{r}(r\theta_r)_r\right], \tag{8}$$

$$u_t+\frac{1}{r}J(u)=\frac{1}{r}\psi_z\left(2\Omega+\frac{u}{r}\right)+\nu\left[u_{zz}+\left(\frac{1}{r}(ru)_r\right)_r\right], \tag{9}$$

$$-\zeta=\frac{1}{r}\psi_{zz}+\left(\frac{1}{r}\psi_r\right)_r, \tag{10}$$

where $J(\ )=\psi_r(\ )_z-\psi_z(\ )_r$ is a Jacobian form of the convective terms.

We wish to obtain solutions for the flow set up by heating the vertical walls, both in the presence and absence of rotation. Both free and rigid upper surfaces will be considered, the latter in Part 2. The variables computed are ψ, θ, u and ζ; the eliminated variables (v, w, p) performed only a secondary and diagnostic function with the vorticity being the central element of flow study in the manner discussed by Lighthill (1963).

Solutions of the equations must satisfy boundary conditions on the planes $z=0$, d and walls $r=a,b$. The vanishing of the normal velocity components along these surfaces necessitates putting the stream function equal to a constant, the value of which will be taken to be zero following a discussion on computational conditions. The boundaries are rigid ones for the walls, base and surface when the latter is in contact with its lid so that the tangential velocity component also vanishes, i.e., the normal derivative ψ_n is zero. For the case of a free upper surface, i.e., the lid not in contact, the tangential stresses on the free surface must vanish, which requires ψ_{zz} to be zero, i.e., the vorticity $\zeta=0$. For the thermal conditions we shall consider only the

case of insulated base and surface, $\theta_z=0$ on $z=0,d$, and constant wall temperatures $\theta=0,1$ on $r=a,b$.

a. Energy and steady state balance requirements. In discussing the results, it will prove useful to refer to the balance requirements for energy, vorticity, temperature variance and total heat transfer. Although the performance of a comprehensive dynamic diagnosis of these balances requires greater calculation, it is considered necessary because an apparent simulation of the physically observed characteristics does not in itself form an understanding. Diagnostic integral techniques provide a very sensitive measure of the mechanical similarity of model to physical entity and may provide the type of insight from numerical studies that is normally derived from analytical studies. For, somewhat in spite of themselves, numerical methods although capable of accounting for nonlinearity and other complexities do not yield an understanding of the mechanisms involved. However, in the integrated form of the equations, the nonlinear effects vanish or are simplified, and make the task of interpretation easier.

In studying the balance requirements we seek to conserve those quantities which are actually conserved in the physical process. It is useful, therefore, to ensure that energy, momentum and mass are strictly conserved by the numerical scheme of solution. When the equations are written in perfectly conserving form, we have available a useful and powerful check on the accuracy of the computation. Furthermore, the degree of balance reached by the energy components indicates the progress made by the computation towards achieving a steady state and provides some confirmation of a proper execution of the computation.

The equation for the kinetic energy prediction is given by multiplying Eq. (7) for the vorticity by ψ and the zonal velocity equation (9) by u and adding the two. Particular use is made of the integrated forms of the energy equations. Thus, denoting the volume integral over the r,z cross section by $\langle\ \rangle$, we can define the kinetic energy total E_k as the sum of the meridional kinetic energy $E_k(\psi)$ and the zonal kinetic energy, i.e.,

$$E_K\equiv\frac{1}{2}\left\langle u^2+\psi\frac{\zeta}{r}\right\rangle,\quad E_K(\psi)\equiv\frac{1}{2}\left\langle\psi\frac{\zeta}{r}\right\rangle. \tag{11}$$

A potential energy integral E_p may be defined as

$$E_p\equiv\beta g\Delta T\langle -z\theta\rangle, \tag{12}$$

in view of the simplified equation of state, and a temperature variance integral, $\sigma_{T^2}\equiv\frac{1}{2}\langle\theta^2\rangle$, may also be formed.

The prediction equations (7)–(9) yield the following system of equations for the time variation of the energy integrals:

$$(E_k)_t=E_k{:}E_p-\epsilon_k, \tag{13}$$

$$(E_p)_t=-E_k{:}E_p-\epsilon_p, \tag{14}$$

$$(\sigma_{T^2})_t=-\epsilon_T, \tag{15}$$

where $E_k{:}E_p\equiv\beta g\Delta T\langle\theta\psi_r/r\rangle=-\beta g\Delta T\langle\psi\theta_r/r\rangle$ represents the gain in kinetic energy by the conversion of potential energy. The diffusive terms are:

$$\epsilon_K\equiv-\nu\left\langle\frac{\psi}{r}\left[\zeta_{zz}+\left(\frac{1}{r}(r\zeta)_r\right)_r\right]+u\left[u_{zz}+\left(\frac{1}{r}(ru)_r\right)_r\right]\right\rangle$$

$$=\nu\left\langle\zeta^2+u_z{}^2+\left(\frac{1}{r}(ru)_r\right)^2\right\rangle, \tag{16}$$

$$\epsilon_P=\beta g\Delta T\kappa\left\langle z\left[\theta_{zz}+\frac{1}{r}(r\theta_r)_r\right]\right\rangle, \tag{17}$$

$$\epsilon_T=-\kappa\left\langle\theta\left[\theta_{zz}+\frac{1}{r}(r\theta_r)_r\right]\right\rangle. \tag{18}$$

Another important integral quantity is the Nusselt number. Two such quantities are considered, one to represent the total outflow of heat through the inner wall (T_a will always be taken as less than T_b in this paper) and one for the inflow of heat through the outer (hot) wall. The Nusselt number measures the effectiveness of the flow as a heat transferring mechanism and is defined relative to the amount of heat transfered by solid conduction under the same temperature difference ΔT. Then

$$\mathrm{Nu}(c)=\left(\frac{c}{d}\log\frac{b}{a}\right)\int_0^d\theta_r(c)dz;\quad c=a,b \tag{19}$$

denotes the inner and outer values, respectively.

A steady state may be defined as occuring when the following conditions are achieved:

E_k, E_p, σ_{T^2} are constant, $E_k{:}E_p=\epsilon_k=-\epsilon_p$, $\epsilon_T=0$, and $\mathrm{Nu}(a)=\mathrm{Nu}(b)=$ a constant value, $\bar{\mathrm{Nu}}$.

b. The numerical method. To yield solutions, the continuous equations are replaced by a finite difference analogue. The variables ψ, ζ, θ and u are located at the same uniformly spaced mesh points in the vertical cross section of the fluid such that there are L spaces of length Δr and M spaces of length Δz at times $n\Delta t$, where n is the time indexing integer. To exhibit the finite difference equations and their multidimensional properties in compact form, we define the following difference and averaging operators in the notation of Richardson (1922) and Lilly (1964)

$$\delta_x\phi\equiv\left[\phi\left(x+\frac{\Delta x}{2}\right)-\phi\left(x-\frac{\Delta x}{2}\right)\right]\Big/\Delta x, \tag{20}$$

$$\bar{\phi}^x\equiv\left[\phi\left(x+\frac{\Delta x}{2}\right)+\phi\left(x-\frac{\Delta x}{2}\right)\right]\Big/2, \tag{21}$$

where ϕ represents a function of the variable $x(\equiv r,z)$ and Δx is the discrete grid interval of x. The bar and delta operators form a linear commutative and dis-

tributive algebra for which various operator rules and identities exist, e.g., Fox (1957).

The velocities are defined at points intermediate to those of the general grid by the relations $rv=-\delta_z\psi$ and $rw=\delta_r\psi$; they satisfy the finite difference analogue of the continuity equation

$$\delta_r(rv)+\delta_z(rw)=0 \tag{22}$$

and are evaluated diagnostically from the stream function.

The governing equations are written in the finite difference forms:

$$\delta_t\bar{\theta}^t+\frac{1}{r}J_4(\theta)=\kappa\left[\delta_{zz}\theta+\frac{1}{r}\delta_r(r\delta_r\theta)\right]_{\text{lag}}, \tag{23}$$

$$\delta_t\bar{u}^t+\frac{1}{r}J_4(u)=\frac{1}{r}\left(2\Omega+\frac{u}{r}\right)\delta_z\bar{\psi}^z+\nu\left[\delta_{zz}u+\delta_r\left(\frac{1}{r}\delta_r(ru)\right)\right]_{\text{lag}}, \tag{24}$$

$$\delta_t\bar{\zeta}^t+J_A(\zeta/r)=-\beta g\Delta T\delta_r\bar{\theta}^{rzz}+2\Omega\delta_z\bar{u}^z+\frac{1}{r}\delta_z\overline{(u^2)}^z+\nu\left[\delta_{zz}\zeta+\delta_r\left(\frac{1}{r}\delta_r(r\zeta)\right)\right]_{\text{lag}}, \tag{25}$$

$$\frac{1}{r}\delta_{zz}\psi+\delta_r\left(\frac{1}{r}\delta_r\psi\right)=-\zeta, \tag{26}$$

where central time differencing is used to ensure stability and where the subscript "lag" on the diffusion terms indicates that they are evaluated non-centrally at time $(n-1)\Delta t$. The multiple averaging of the buoyancy term is necessary to make the energy conversion term $E_k:E_p$ the same when given by kinetic energy and potential energy equations. The particular forms of the convective terms,

$$J_4(\phi)=\delta_z(\bar{\phi}^z\delta_r\bar{\psi}^{rz})-\delta_r(\bar{\phi}^r\delta_z\bar{\psi}^{rz}), \tag{27}$$

$$J_2(\phi)=\delta_r\overline{(\psi\delta_z\bar{\phi}^z)}^r-\delta_z\overline{(\psi\delta_r\bar{\phi}^r)}^z, \tag{28}$$

$$J_A(\phi)=\tfrac{2}{3}J_4(\phi)+\tfrac{1}{3}J_2(\phi), \tag{29}$$

are so chosen because of their stability characteristics.

c. Stability considerations. In the numerical integration of the difference equations, consideration of the stability of numerical system is essential. The method being used is an acknowledged stable one when subject to the usual (linear) advection and diffusion time step requirements. The approximated equations allow the existence of only internal gravity waves because the Boussinesq approximation filters out sound waves and the enforced constant surface height filters out surface gravity waves. In practice, the diffusive requirement that the time step Δt be less than $\Delta_{z,r}^2/8\nu$ was used as frequently as the internal gravity wave requirement that $\Delta t<\Delta_{z,r}/(2\beta gd\Delta t)^{1/2}$, as given by the Brunt-Väisälä frequency.

The instability associated with the aliasing of nonlinear terms and fictitious build-up of energy when integrations over an extended period are involved [see Phillips (1959)] is avoided by the choice of advective forms $J_4(\phi)$, $J_A(\phi)$. The Jacobian $J_4(\phi)$ conserves temperature variance, zonal velocity and zonal kinetic energy, whereas the form $J_A(\zeta/r)$ conserves vorticity squared and the meridional kinetic energy (Lilly, 1964). By conservation, we mean that the difference summation and the corresponding continuous volume integral of the Jacobian reduce to the same value, usually zero. Thus, it appears that the difference technique and corresponding quadrature technique must consistently satisfy Stokes's theorem in the same manner as the continuous system.

The tendency for central time differencing to lead to a slow splitting of variables at adjacent time steps was removed by periodically averaging the variables of two adjacent time steps. This is an instability in the time variable compared with the space mode instability removed in the Jacobian situation.

d. Balance requirements in difference form. Although the core of the conserving problem lies with the advection Jacobian terms, to be consistent, the finite difference energy equations must be derived from the finite difference prediction equations. Proceeding as for the continuous case, we obtain for kinetic energy the expression

$$\bar{E}_K^t=\frac{1}{2}\left[\tilde{u}\tilde{u}^t+\frac{1}{r^2}\widetilde{(\delta_z\psi\delta_z\psi)}^{tz}+\frac{1}{r^2}\widetilde{(\delta_r\psi\delta_r\psi)}^{tr}\right], \tag{30}$$

where

$$uu^t\equiv u\left(t+\frac{\Delta t}{2},r,z\right)\cdot u\left(t-\frac{\Delta t}{2},r,z\right),$$

and the square parentheses [ ] represents the quadature over all grid points. The energy conversion term, as derived from the potential energy difference equation, takes the form

$$E_K:E_P=-\beta g\Delta T\left\langle\frac{z}{r}J_4(\theta)\right\rangle=\beta g\Delta T\left\langle\frac{\bar{\theta}^{zz}}{r}\delta_r\bar{\psi}^r\right\rangle, \tag{31}$$

so that the buoyancy term which gives rise to this term via the kinetic energy equation must be multiply-averaged.

The quadrature equations which correspond to the energy integrals of the continuous system are:

$$\delta_t\bar{E}_K^t=E_K:E_P-\epsilon_K, \tag{32}$$

$$\delta_t\bar{E}_P^t=-E_K:E_P-\epsilon_P, \tag{33}$$

$$\delta_t\sigma_{T^2}=-\epsilon_T, \tag{34}$$

where

$$E_P = -\beta g \Delta T[z\theta], \tag{35}$$

$$\sigma_{T^2} = \tfrac{1}{2}[\tilde{\theta}\theta]^t, \tag{36}$$

$$\epsilon_K = -\nu\left\{\frac{\psi}{r}\left[\delta_{zz}\zeta + \delta_r\left(\frac{1}{r}\delta_r(r\zeta)\right)\right]_{\text{lag}} + u\left[\delta_{zz}u + \delta_r\left(\frac{1}{r}\delta_r(ru)\right)\right]_{\text{lag}}\right\}, \tag{37}$$

$$\epsilon_P = \beta g \Delta T \kappa\left[z\left(\delta_{zz}\theta + \frac{1}{r}\delta_r(r\delta_r\theta)\right)_{\text{lag}}\right], \tag{38}$$

$$\epsilon_T = -\kappa\left[\theta\left(\delta_{zz}\theta + \frac{1}{r}\delta_r(r\delta_r\theta)\right)_{\text{lag}}\right]. \tag{39}$$

Quantities analogous to kinetic energy and variance are formed which involve cross products at adjacent time steps, defined above by the tilde operator. These quadratures are relevant to the continuous integrals only if the solution behaves smoothly in time and the splitting instability is avoided.

Boundary placement and conditions must be considered in forming the quadratures as some computational conditions are required for the definition of certain integrals at the boundary points. In a grid system, the boundary can be placed either at a grid point or between two points. Although there is no explicit reason for placing the boundary at a grid point in this problem, such a choice made the solution of the Poisson equation more convenient and gave greater overall consistency.

Computational conditions arise because one-sided difference forms of the prediction equations are required at the boundary points to ensure conservation of the integrals. However, this form of the prediction equation is not used as boundary conditions are available. To overcome the problem caused by this discrete quantization of the fluid into cells, the definition of the quadrature requires extra conditions to conserve the integrals. In the annulus problem, the presence of strong diffusive boundary layers necessitates the mutual conservation of both the diffusive and advective terms, not just the advective terms, as is normally the case.

To see how the computational conditions are derived, consider for convenience a transfer equation in one dimension x, i.e.,

$$\theta_t + (\theta v)_x = \kappa\theta_{xx}. \tag{40}$$

Applying this equation to the grid points of x, say $i=1,2,\ldots L+1$, we obtain at $i=1$ the necessary equation conserving the quadrature namely,

$$\delta_t\bar{\theta}_1^t + \frac{1}{\Delta x/2}[(\bar{\theta}^x\bar{v}^x)_{1\frac{1}{2}} - (\bar{\theta}^x\bar{v}^x)_1] = \frac{\kappa}{\Delta x/2}[(\delta_x\theta)_{1\frac{1}{2}} - \theta_1'], \tag{41}$$

where the derivative on the boundary θ_1' has yet to be defined. As the boundary condition $\theta_1 = \text{constant}$ is supplied, this equation must be satisfied identically. This requirement provides a definition of

$$\theta_1' = (\delta_x\theta)_{1\frac{1}{2}} - \frac{\Delta x}{2\kappa}[(\bar{\theta}^x\bar{v}^x)_{1\frac{1}{2}} - (\bar{\theta}^x\bar{v}^x)_1]. \tag{42}$$

In two dimensions, a direct extension of this idea yields definitions of gradients at the boundaries for use in the Nusselt and ϵ_p, ϵ_T integrals. As a corollary, the boundary condition $\theta_1' = \text{constant}$ requires that the prediction equation be used to predict θ_1; the assumption sometimes made that $\theta_1 = \theta_2$ is inconsistent with this approach. The need for the above type of condition on the boundary vorticity in the integral E_k can be avoided simply by taking $\psi = 0$ as the boundary condition.

e. Numerical procedure. In executing the calculation, u and θ can be directly evaluated from values at the previous time step. Similarly, we can predict the interior vorticity values from which the stream function can be updated on solving the Poisson equation. It then remains to evaluate new vorticity values for the boundary. These boundary values are required for calculating the adjacent interior frictional terms. They are obtained by reversing the rôle of the Poisson equation. To solve the Poisson equation at the boundary with the same degree of accuracy as it is solved in the interior region, a higher order formula must be used. The derivation of such a higher order formula has been given by Pearson (1965). For the base, this takes a form

$$\zeta_{i1} = -\frac{1}{r}\psi_{zz} = \frac{1}{r\Delta_z^2}[3.5\psi_{i1} + 0.5\psi_{i3} - 4\psi_{i2} + 3\Delta_z(\psi_z)_{i1}] + O(\Delta_z)^2, \tag{43}$$

which allows the non-slip boundary condition $\psi_z = 0$ to be introduced into the system. The non-slip velocity condition does not enter the stream function solution directly but enters via the concurrent vorticity field, Eq. (43). This form of calculation reflects the physical behavior of how a boundary determines the flow in the fluid interior; for a discussion of this see Lighthill (1963).

The actual integration of the Poisson equation to give the stream function at each time step was made by a trigonometric interpolation method. This method is more time consuming than the standard Liebmann accelerated relaxation method, but has the advantage of being more accurate than the Liebmann method with its associated spurious truncation errors. It is also exact for the finite difference scheme. The method is based on writing the function in terms of a trigonometric series whose coefficients become the new unknowns, i.e.,

$$\psi_{ij}{}^n \equiv \sum_{k=1}^{M-1} A_{ik}\sin\left[\frac{\pi k}{M}(j-1)\right]. \tag{44}$$

This expression automatically satisfies the boundary conditions at the base and surface. We express the vorticity in a similar series of known coefficients as

$$\zeta_{ij}^{n} \equiv \sum_{k=1}^{M-1} B_{ik} \sin\left[\frac{\pi k}{M}(j-1)\right]. \tag{45}$$

Upon substituting Eqs. (44) and (45) into the Poisson equation, we obtain a difference equation,

$$A_{i+1k}a_i - A_{ik}b_{ik} + A_{i-1k}c_i = -B_{ik}, \tag{46}$$

where

$$\left.\begin{aligned} a_i &= 1/(\Delta r)^2\left(r+\frac{\Delta r}{2}\right), \quad c_i = 1/(\Delta r)^2\left(r-\frac{\Delta r}{2}\right) \\ b_{ik} &= a_i + c_i + \frac{2}{r(\Delta z)^2}\left(1-\cos\frac{\pi k}{M}\right) \end{aligned}\right\}, \tag{47}$$

which can be solved by Richtmyer's (1957) iteration method.

3. Discussion of numerical solutions

In the problem being considered, there exist small but important boundary layers, the correct description of which is important for an understanding of the overall properties of the flow. The boundary layers, therefore, must be sufficiently resolved for the heat and momentum transfers to be accurately given.

The two parameters, the Rossby and Taylor numbers

$$\pi_4 = (\beta g d \Delta T)/[\Omega^2(b-a)^2], \quad \pi_5 = 4\Omega^2(b-a)^5/(\nu^2 d), \tag{48}$$

have been found by Fowlis and Hide (1965) to be the most useful parameters for describing annulus flow. Although flows with boundary layers can be dealt with, the resolution limit set by the machine capacity restricts the range of π_4, π_5 values over which computation can be meaningfully made. In this paper, calculations were made with the condition that at least 3 grid points should be located within each boundary layer and the accuracy of the results was checked by varying the resolution. The accuracy of those solutions which utilized the entire machine could only be estimated by re-performing part of the calculation with a coarser grid. The use of high resolution grids and the requirement of 3 points to the boundary layer seemed to be adequate for producing reliable solutions. Veronis (1966) found that to obtain reliable results in a similar system, it was sufficient to have only one grid point within the boundary layer.

Calculations were made with a uniformly spaced grid. It may be advantageous in future calculations to take additional points near the boundaries, but in the present computations, the aim was one of achieving fairly high resolution throughout the whole fluid in order to investigate the extent of the penetration of boundary layer effects into the interior regions of the fluid. The secondary cell systems associated with the sidewall layers and the separation of the boundary layer from the outer wall are examples of such interior region phenomena requiring high resolution. Now that the types and extent of the internal structures are known, a graded mesh would be useful in further studies, provided that the higher resolution did not bias the boundary layer flow in any way.

a. Computational range. Fowlis and Hide (1965) have examined experimentally the effect of various physical parameters such as viscosity or geometry upon the transition criteria. The results show that the principal properties of the flow depend largely on the dimensionless parameters π_4, π_5, $\pi_2 \equiv d/(b-a)$ the aspect ratio, and the Prandtl number $\pi_6 \equiv \nu/\kappa$. The position of the transition between the upper symmetric region and the steady waves regime can be plotted in a π_4 versus π_5 diagram and a transition curve drawn through the points. There is only a slight spread of points about the line which is due to variations in other factors, in particular, low π_2 values. On the other hand, the transition between the lower symmetric and the steady wave regimes forms a straight line on a $\pi_4\pi_6$ versus $\pi_2\pi_5$ diagram.

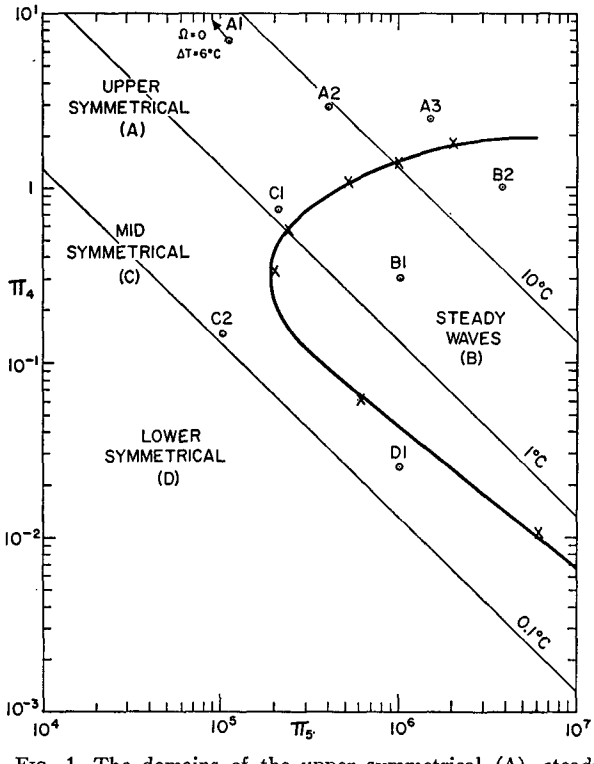

FIG. 1. The domains of the upper symmetrical (A), steady waves (B), mid-symmetrical (C) and lower symmetrical (D) flow regimes in a typical regime diagram. The transition curve separating the symmetric and steady waves regime was obtained by Fowlis and Hide (1965) for experiments under physical system FH, (see Table 1) at the points marked by a cross. The lettered circles denote positions for which numerical solutions were obtained. $\pi_4 \equiv (\beta g \Delta T d)/[\Omega^2(b-a)^2]$ and $\pi_5 \equiv [4\Omega^2(b-a)^5]/(\nu^2 d)$.

TABLE 1. Structure of cases computed. Only cases A3 and B2 are discussed in this paper.

Case	Physical system	Surface condition	Number of grid intervals in r, z	ΔT (°C)	Ω (rad sec^{-1})	π_4	π_5
A1	BE	Fixed	40×40	6.0	0.000	—	—
A2	FH	Fixed	40×60	9.0	0.700	2.863	4.079×10^5
A3	FH	Free	40×80	29.0	1.342	2.510	1.500×10^6
B1	FH	Fixed	40×40	2.3	1.100	0.296	1.010×10^6
B2	FH	Free	40×80	29.0	2.125	1.001	3.759×10^6
C1	FH	Fixed	40×40	1.2	0.500	0.748	2.080×10^5
C2	FH	Fixed	40×40	0.1	0.350	0.127	1.020×10^5
D1	FH	Fixed	40×40	0.2	1.100	0.026	1.010×10^6

System BE: $a=3$ cm, $b=5$ cm, $d=10$ cm, $\nu=0.941\times10^{-2}$ cm^{-2} sec^{-1}, $\kappa=1.420\times10^{-3}$ cm^2 sec, $\beta=2.380\times10^{-4}$ (°C)$^{-1}$, $\bar{T}=23$C, $\pi_6=6.58$.
System FH: $a=3.48$ cm, $b=6.02$ cm, $d=5$ cm, $\nu=1.008\times10^{-2}$ cm^{-2} sec^{-1}, $\kappa=1.420\times10^{-3}$ cm^2 sec, $\beta=2.050\times10^{-4}$ (°C)$^{-1}$, $\bar{T}=20$C, $\pi_6=7.19$.

For a constant geometry and Prandtl number, a single transition curve may be drawn. Such a curve is shown in Fig. 1 for an annulus which has a height equal to twice the width between its walls. This geometry was chosen for computational use because $\pi_2=2$ is the lowest value of the aspect ratio for which observations were recorded in the Fowlis and Hide (1965) experiments. A low aspect ratio is preferable from the computational point in order that the resolution may be made as high for both width and height. Although an aspect ratio of 1.0 would be ideal from the numerical view point, experimentally a higher aspect ratio has been favored 1) for easier control of the apparatus, 2) to produce a similar ratio of Ekman layer to total depth as for the atmosphere, and 3) for values of $\pi_2>2$, the transition between regimes is independent of the actual depth of the fluid.

The cases computed were located at a variety of π_4, π_5 points in the observed transition diagram (Fig. 1), so as to give an idea of the types of flow existing in each region. The cases considered are marked in Fig. 1 by letters corresponding to the region in which they lie. The cases all lie above the line $\Delta T=0.1$C which is the observational limit. Furthermore, the Boussinesq approximation is only accurate up to values of $\Delta T=10$C so that the two flows A3 and B2 can only be regarded as physically correct to a first approximation. The resolution is adequate for cases lying between $\Delta T=0.1$C and 10C and the upper symmetric regime cases A3 and B2 are at the practical limit of 40×80 points.

With the exception of cases A3 and B2, all other flows are treated as having a rigid surface and will be reported in a subsequent paper. It should be noted that the transition curve is that of a free surface fluid. The lower symmetric regime computations were made for a flow with a rigid surface in order to provide a direct comparison with Robinson's (1959) theory for that regime. The upper symmetric cases A3 and B2 (free surface flows) were made, despite resolution and Boussinesq limitations, in order to examine the flow on both sides of the transition curve in a region in which π_4 appears to tend to the constant value predicted by baroclinic instability theory. This region should therefore be one of minor boundary layer influence.

An additional case A1 (with a zero rotation rate) was calculated. This case was made identical to that of an experiment, comprehensively reported by Bowden and Eden (1965), for which such details as the temperature field structure are given. This and other experiments reported by Bowden and Eden (1965) all have a high aspect ratio of 5 so that only one of their experiments was duplicated for testing the numerical solution and technique. Details of the cases calculated are summarized in Table 1.

b. Initial conditions and computational procedure. The numerical integrations were all performed in the same way. At time $t=0$ the initial state of the fluid was assumed to be one of isothermal solid rotation at a temperature of 20C. At this instant, the temperature differential across the fluid is imposed by altering the wall temperatures in such a way that their average value remains at 20C. (The one exception is case A1, the mean temperature in this instance being 23C with the appropriate physical constants of that temperature being used.) Thus, at $t=0$, we have $\psi(r,z,0)=\zeta(r,z,0)=u(r,z,0)=0$ for all r, z and $\theta(r,z,0)=0.5$, $\theta(a,z,0)=0$, $\theta(b,z,0)=1$. Then, with the appropriate time step increment, integrations were made until the fluid system evolved into a steady state of balance. In every calculation the flow eventually became steady.

When the forces attain a balance, the various energy integrals become constant. In practice, we therefore define the steady state to be realized when the kinetic energy integral is constant and the two Nusselt numbers lie within a few per cent of each other. The diffusive elements determine the time taken to attain the steady state. The thermal components usually reach a steadiness later than the kinetic elements and the balancing of the Nusselt numbers constitutes an extremely sensitive indicator of the degree of balance reached, whereas the kinetic energy integral is an insufficient measure. A typical approach to the steady state is shown in Fig. 15 where the integrals are plotted against time for case A3.

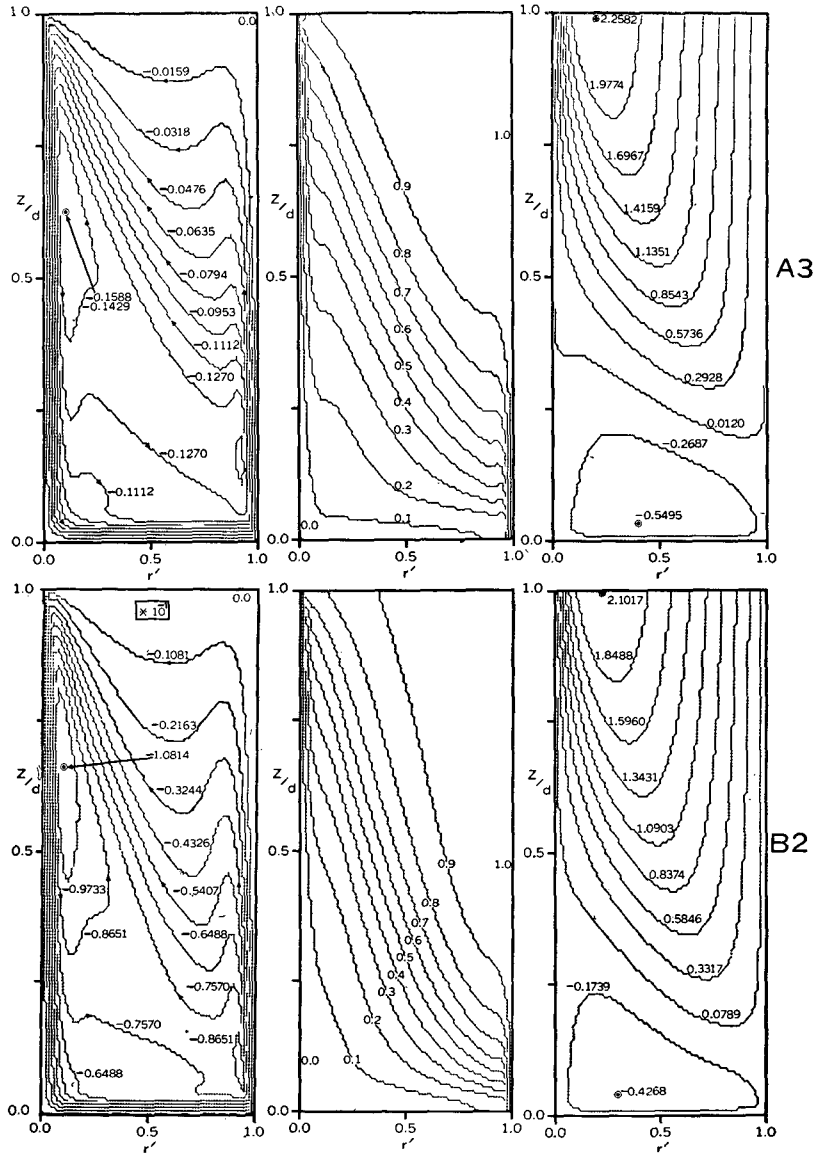

FIG. 2. The steady state contours of stream function, normalized temperature and zonal velocity for free surface flows A3 and B2 (see Table 1). Stream function arrows indicate flow direction and positive zonal velocities indicate westerly flow, all in cm sec^{-1}. Extreme magnitudes of zonal velocity and stream function are marked. $r' \equiv (r-a)/(b-a)$, the non-dimensional radial coordinate, commences at the inner cylinder (left of diagram).

In certain instances, the above type of integration was made with a given grid and its steady state solutions used as the initial state for a further integration for a grid with double the previous resolution. Such an approach succeeded in saving time only if the coarser grid gave a steady state solution close to that given by the finer grid. At various time stages, contour plots of the streamline pattern, the zonal isotachs, the isotherm pattern and vorticity were made, and these will be used in presenting the results.

c. Solutions of the two free surface cases. The steady state solutions of the two free surface cases A3 and B2, presented in Fig. 2, are qualitatively similar. They differ from each other only in their rotation rates. According to observation (directly applicable in this instance) A3 should lie in the upper symmetric regime and B2 in the steady waves regime. The effects of having a free surface are examined by comparing these flows with that of the rigid surface case A2 which will be presented in Part 2.

1. Meridional flow. The stream function contours of Fig. 2 show a meridional flow made up of a direct (Hadley) cell and two weaker secondary cells. The direct cell flows through boundary layers on the inner cylinder and base and, to a lesser extent, on the outer cylinder. Unlike the rigid surface flows, the free surface

cannot maintain a boundary layer so that the meridional flows of the free and rigid surface systems differ. In fact, free surface flows resemble a distorted version of the rigid surface flow. Because the free surface cannot viscously support a flow along it, the upward moving fluid leaves the outer cylinder, falls under gravity, and then flows up and across the interior section of the annulus, where it completes the circuit by being entrained into the boundary layer on the inner cylinder. The region of maximum transport occurs near the middle of the inner cylinder, whereas in rigid surface flows this region is located near the bottom of the outer cylinder.

The secondary system is made up of 2 interior cells, one associated with the hot wall boundary layer, and the other with the cold wall boundary layer. These cells strengthen the mass transport near the wall. The countercurrent cell is much smaller on the outer cylinder than on the inner; this difference contrasts with the equal cells of rigid surface flows. The inner cylinder cell, strengthened by the interior cross flow, tapers toward the top. Faller (1958) has observed the meridional flow structures of flows with a free surface and his radial velocity profiles agree qualitatively with that of case A3, presented in Fig. 3. The maximum of mass transfer occurs in the boundary layer along the base, and is compensated for by an almost constant return flow.

2. Temperature field. The distinctive features of the isotherms of A3 and B2 lie in their pronounced linearity over the fluid interior, and in their concentration into thermal boundary layers over short and narrow sections of fluid near the cylinders. In case A3, approximately one-fourth of the fluid lies at almost constant temperature in a very stable region between the 0.9 and 1.0 isotherms. The larger rotation rate of B2 causes the isotherms to slope more vertically and form smaller thermal boundary layers for that case. The streamlines of B2 also slope more strongly than those of A3 in keeping with the tendency of the fluid in the interior to flow parallel to and along isotherms.

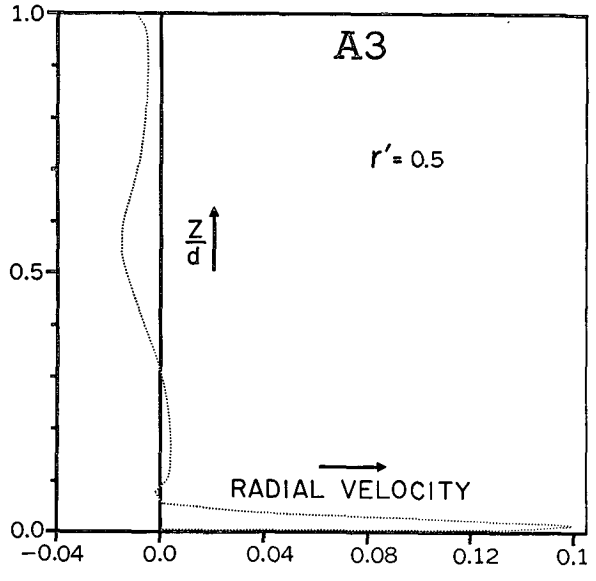

FIG. 3. A typical vertical distribution of radial velocity for a free surface flow (A3). Values are in cm sec^{-1} in a plane midway between cylinders.

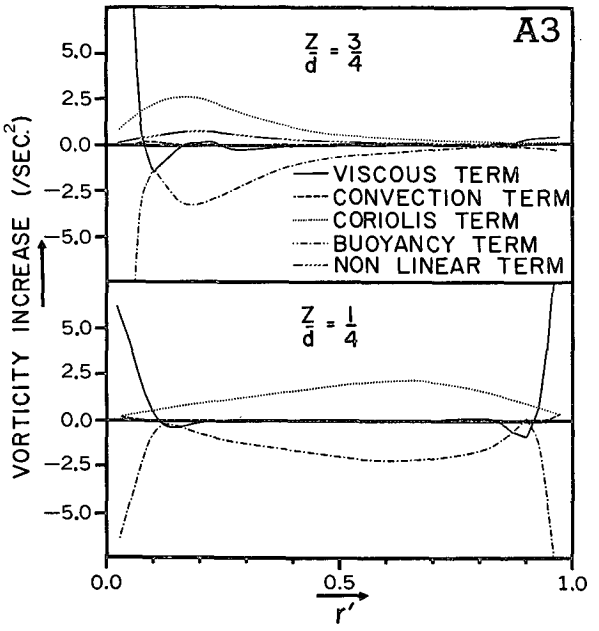

FIG. 4. Representative radial distributions of the forces contributing to the balance of terms in the vorticity equation for flow A3 at heights of $d/4$ and $3d/4$. For the meaning of the terms, consult the vorticity prediction equation (7). Geostrophic balance of the interior is indicated.

3. Zonal flow. The zonal flow consists of westerly flow in the upper three-fourths of the annulus and easterly flow near the base: by westerly flow we mean flow in the same sense as the rotation. The maximum westerly flow reaches a value roughly 4 times that of the maximum easterly. This contrasts with the equal extent and extrema of westerly and easterly flow in rigid surface flows. The maximum westerly flow occurs at the core of a jet stream type of flow on the fluid surface near the point $r'=1/4$. The line separating the east-west flow, $u=0$, inclines upward toward the inner cylinder even more so for the flow with the larger rotation rate. Bowden and Eden (1965) have observed similarly shaped conical regions of zonal flow. The constant temperature of the upper region produces zonal isotachs which lie parallel to the outer cylinder.

4. Vorticity balance. One of the assets of a numerical solution is that one can study the balance of terms in the equations at each point of the system. The forces balancing in the vorticity equation are shown in Fig. 4 at $z'=1/4$ and $3/4$. These are typical radial variations and the meaning of the terms may be grasped from Eq. (25). Although the interior region of the fluid lies in a balance between the Coriolis term $2\Omega u_z$ and the buoyancy term $-\beta g\Delta T\theta_r$, i.e., a geostrophic balance, the non-linear term $(u^2/r)_z$ makes a significant contribution to the vorticity balance in the upper half of the fluid.

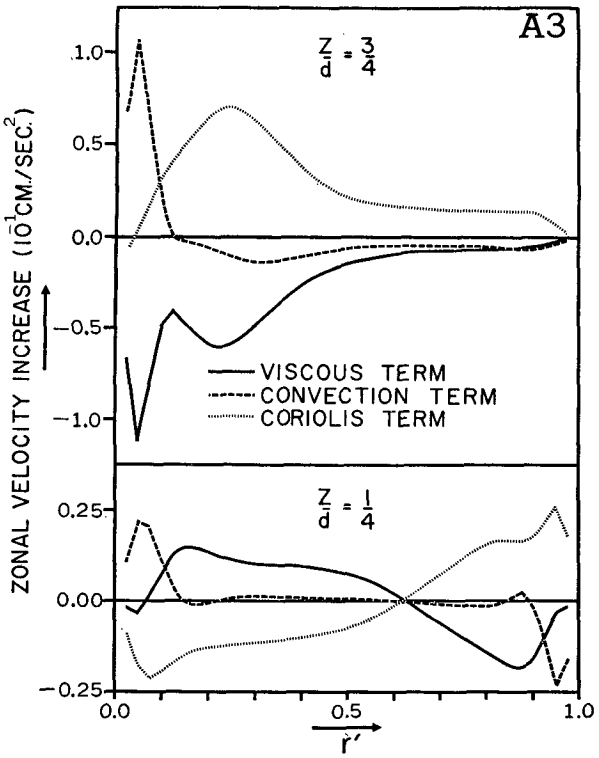

FIG. 5. Representative radial distributions of the forces contributing to the balance of terms in the zonal velocity equation for flow A3 at heights of $d/4$ and $3d/4$. Note the different scales used and lack of convection in the fluid interior.

In the boundary layers on the cylinders, the vorticity components constitute a balance between the buoyancy term $=\beta g\Delta T\theta_r$ and the friction term $\nu[\zeta_{zz}+(1/r(r\zeta)_r)_r]$. The buoyancy force vanishes in the upper half of the fluid near the outer cylinder because of the region of constant temperature that occurs there. Thus, no boundary layer exists in that region.

5. Zonal velocity balance. The components of the zonal velocity equation, Fig. 5, exhibit a balance between the Coriolis term, $-2\Omega v$, and the viscosity term, $\nu[u_{zz}+(1/r(ru)_r)_r]$. The non-linear term uv/r being negligible, is absent.

The boundary layers on the lower part of the cylinders exist under a balance between the Coriolis term $-2\Omega v$ and the convection term $-r^{-1}J(u)$ of the zonal velocity equation. However, in the upper half the boundary layer on the inner cylinder, the viscous term $\nu[u_{zz}+(1/r(ru)_r)_r]$ replaces the Coriolis term in the balance. As noted in the vorticity balance, no boundary layer exists on the upper half of the outer cylinder.

It is important to note the vanishing of the zonal friction term at all parts of the side walls except the upper part of the inner cylinder. This implies that the angular momentum and kinetic energy have a sink region of dissipation only on one limited part of the container, namely on the upper half of the inner cylinder, close to the jet stream. A single source region occurs over the base of the annulus. The absence of a momentum source at the hot wall indicates that this potentially greatest source does not contribute to the general fluid structure; this is not true, however, of the transient flow as will be seen later.

The picture that these facts suggest is one in which the meridional circulation transports the momentum generated by the easterlies at the base, upward and inward to the top of the inner cylinder. There the flow down the wall dissipates the momentum. A composite diagram of the stream function and the zonal isotachs (Fig. 7) indicates that the fluid flows across the jet stream in most regions. The strongest regions of meridional momentum transport uv occur in the uppermost part of the boundary layer on the inner cylinder (the momentum sink region) and in the boundary layer along the base and in the upward sloping streamlines of the interior.

6. Heat balance. The component terms of the temperature equation (Fig. 6) confirm that the flows A3 and B2 are essentially along or parallel to the isotherms. Heat transfer by conduction is significant only in the small thermal boundary layers. In the interior, the convection conveys the heat inward and upward with a balance between the so-called horizontal convection term $-(v\theta)_r$ and vertical convection term $-(w\theta)_z$.

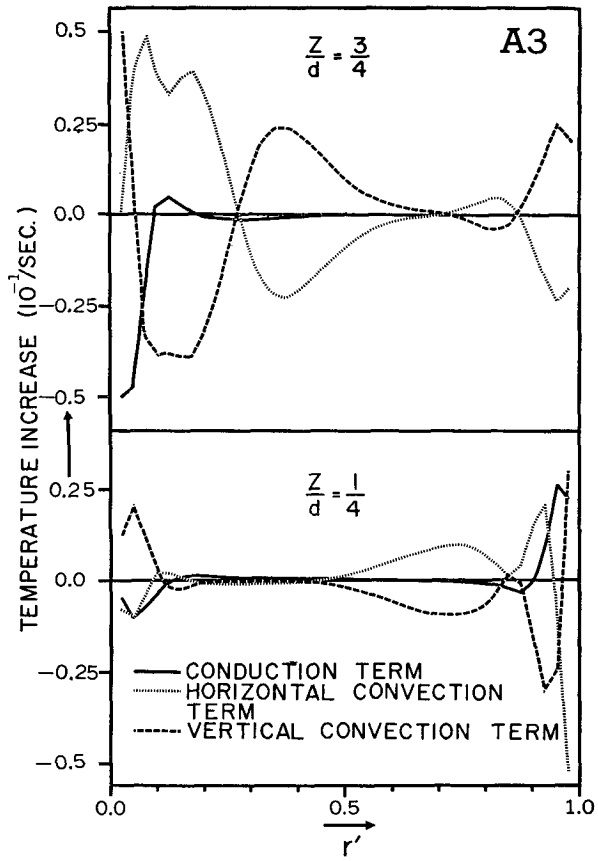

FIG. 6. Representative radial distributions of the balancing terms of the normalized temperature equation for flow A3 at 2 heights. Notice the lack of conduction in the interior.

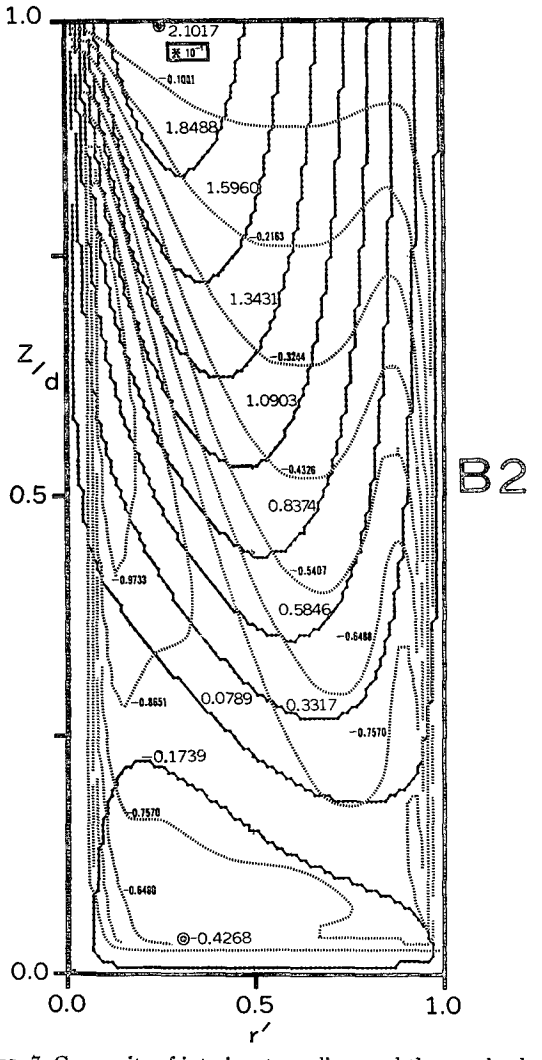

FIG. 7. Composite of interior streamlines and the zonal velocity contours of flow B2 illustrating their interaction and momentum transport (see text for further discussion).

The steady state Nusselt numbers given by the solutions of A3 and B2 are 8.25 and 5.30, respectively. Thus, the Nusselt number is proportional to Ω^{-1}, to within 2 per cent for these two experiments. This clearly indicates the way in which rotation inhibits the heat transfer properties of a free surface fluid in the convective regime.

7. Analogue implications. A side issue of the present study is the question of what conclusions can be drawn from the solution of the axisymmetric flow toward explaining the resemblance between the more complex annulus flows and the atmosphere. The cases being considered (A3 and B2) have parameter values approaching those applicable to the atmosphere.

On the structural side, the temperature fields obtained resemble the potential temperature distribution in the atmosphere. Although the annulus system is heated from the side walls, the flow so arranges itself that the heating and cooling are isolated to two limited regions in the vicinity of the bottom of the hot wall and top of the cold wall. The atmosphere possesses a complex heating structure in which the earth's surface plays a crucial rôle. However, the atmospheric heat source and sink are, as far as the dynamics are concerned, located at the equatorial surface and polar tropopause, so there is some similarity, albeit over-simplified. The momentum balance and flow structure of the two systems are different. However, allowing for the enforced axisymmetry of the solutions, the results may then be justifiably compared to the zonally symmetric solutions obtained for atmospheric flow prior to its being disturbed [see Smagorinsky (1963)]; as such there exist basic similarities between both flow systems in that both have easterlies at the base and westerlies in the upper fluid, and similar meridional flow and temperature patterns.

To assess the role of the boundary layers in forming the flow features, we examine the energy transformation integral $E_k:E_p$. This integral describes the transformation of potential energy into kinetic energy, the basic mechanism that maintains the flow in the annulus. The sidewall boundary layers and the interior cross flow contribute the greater part of the integral $E_k:E_p$. The radial distribution of the contributions to the integral (Fig. 8) shows that the boundary layer contributions oppose each other. If the boundary layers are mutually compensating as energy mechanisms, as Fig. 8 indicates, then the analogy of annulus to atmosphere improves. A significant conversion of potential energy into kinetic energy is accomplished by the fluid in its motion from the outer cylinder to the inner one, rising as it does along paths less inclined to the horizontal than the isotherms.

A direct examination of the stability of the flows A3 and B2 to see if the symmetry is physically real, would involve excessive additional computation. Instead, we examine the stability with the aid of the criterion

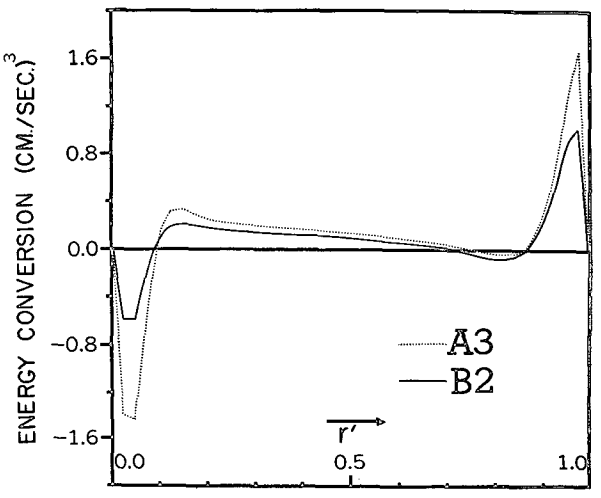

FIG. 8. Radial composition, $\beta g \Delta T \int_0^d \theta w dz$, of the potential energy conversion to kinetic energy, $E_K:E_P$. This integral is weighted by r in forming the net conversion.

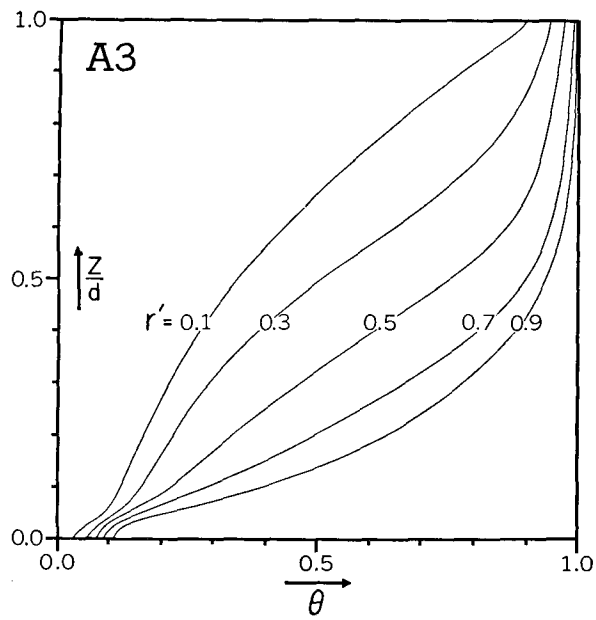

FIG. 9. The vertical distribution of normalized temperature at non-dimensional radii, $r'=0.1$, 0.3, 0.5, 0.7 and 0.9, for flow A3.

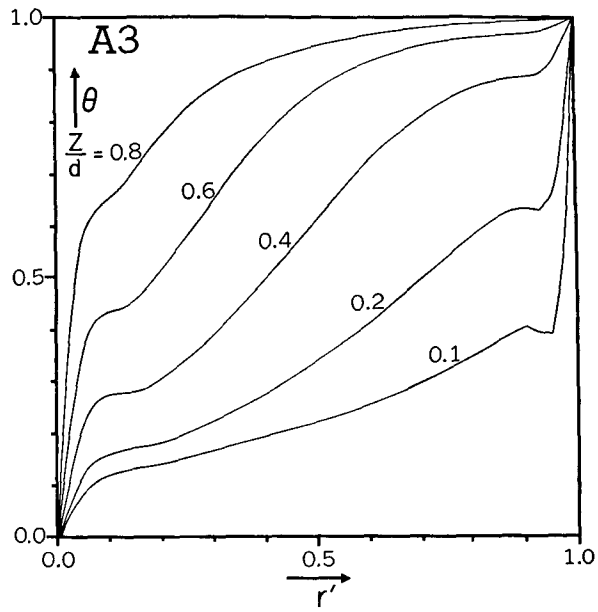

FIG. 10. The radial distribution of normalized temperature at normalized heights of 0.1, 0.2, 0.4, 0.6 and 0.8, for flow A3.

derived by Eady (1949). Use of this criterion presupposes that the instability is geostrophic baroclinic instability, that the boundary layers play no part in the process, and that the idealizations of Eady's model befit the annulus. The assumptions of the model are: that viscosity and thermal conduction can be ignored; the impressed horizontal and vertical temperature gradients are constant, which with the geostrophic assumption gives a basic zonal flow of uniform vertical shear; the curvature is unimportant; the thermal Rossby number defined as $\theta_r\pi_4$ is much less than 1/4; and the slope of the isotherms is of the order of this number multiplied by $d/(b-a)$. Under these assumptions, linear perturbation theory states that the basic flow is stable or unstable to small-amplitude wave-like disturbances according as to whether the normalized temperature gradient, $\sigma_z \equiv T_z/(\Delta T d)$, exceeds or falls short of the value $2.32/\pi_4$.

Thus, the flow remains stable when the vertical temperature gradient induces sufficient vertical static stability to overcome the instability caused by the zonal shear associated with the horizontal temperature difference.

Examination of the criterion from cases A3 and B2 is most conveniently made by reference to Figs. 9, 10, 11, and 12, which show separately the temperature variation with r and z. The condition of constant temperature gradient holds only in the interior region. Assuming the criterion applies, the condition for case A3 to be a stable flow is that θ_z exceed 0.9. This stipulation is complied with over that part of the fluid interior where σ_z can be regarded as constant. However, if σ_z is evaluated as the mean temperature difference between surface and base, its value at 0.88 is less than the critical value. The large isothermal layer near the free surface causes this reduction in σ_z. This indecisiveness suggests that case A3 is a stable flow lying close to the actual transition curve. This fact is in keeping with observation. The critical value for case B2 is 2.3. The flow is definitely unstable as σ_z has an overall mean value of 0.8 and localized values which exceed the critical value only in a small region near the outer wall boundary layer. Thus, the flow B2 is definitely unstable according to Eady's criterion.

The solutions suggest that the instability depends on the quantitative, not qualitative, properties of the flow. However, there are some qualitative differences. Flow B2 has a more variable vertical temperature field (Fig. 11) than flow A3 (Fig. 9) and exhibits little of the latter's linearity. It is interesting to compare both these distributions with the temperature profiles of a fixed surface experiment A2 shown in Fig. 13. The profiles of the fixed surface flow exhibit far less variability and the static stability is almost constant throughout the fluid. The effect of the variability of temperature gradient upon the stability characteristics is still unknown. It has been suggested that radial variations in the vertical gradient of the isotherms in the annulus could function in the same way as the variations of the Coriolis parameter do in the atmosphere.

8. Accuracy. The accuracy of the solutions is most conveniently examined by comparing the values of the various integral quantities as given by the actual grid system, (40×80) points, and by a coarser grid, (30×60) points, at an identical stage in the integrations, i.e., 21.5 sec (or approximately 7 annulus days). The ratio of the (30×60) to (40×80) values of the E_k, $E_k(\psi)$, $E_k{:}E_p$, ϵ_k, Nu(a) and Nu(b) integrals are, respectively, 1.062, 1.040, 1.066, 1.018 and 1.013. This indicates a maximum difference of 7 per cent between

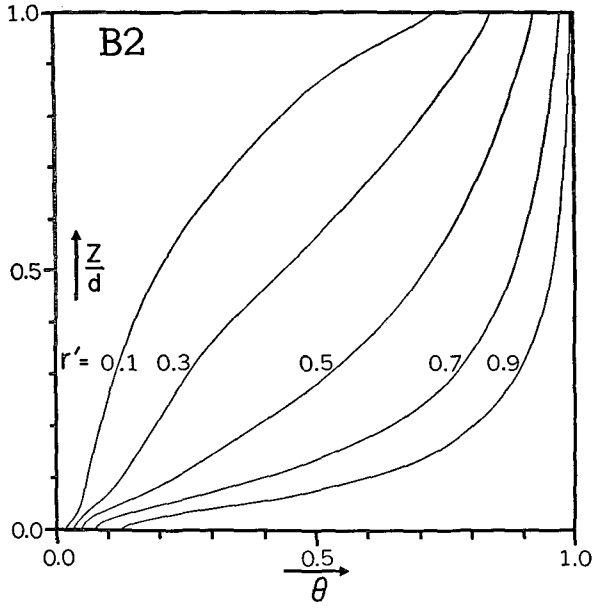

FIG. 11. Same as Fig. 9 for flow B2.

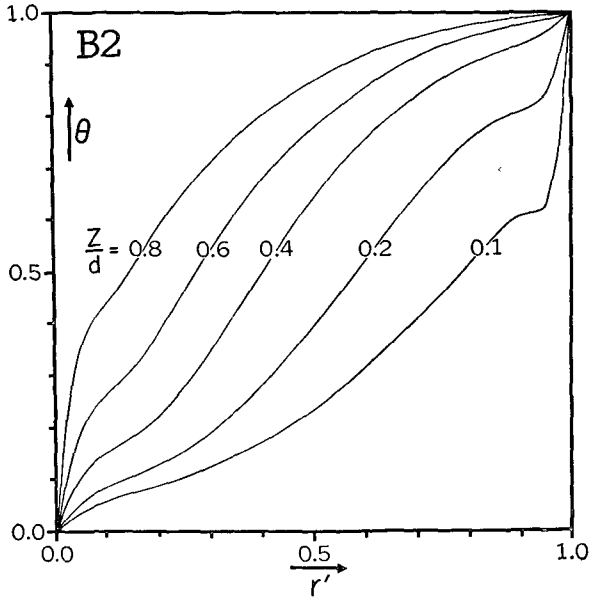

FIG. 12. Same as Fig. 10 for flow B2.

the solutions so that the 40×80 solution is probably accurate.

d. Transient aspects of the solutions. A feature of the technique of integrating to a steady state in discrete time steps is that the intermediate flow fields are given as a by-product of the calculations. A set of the evolving flow patterns of case A3 (Fig. 14) is given at those instances which best illustrate the essential stages of growth. Time graphs (Fig. 15) of the various integral expressions aid the discussion of the flow changes.

1. $t=1.5$ sec. The imposed initial conditions are responsible for the concentration of isotherms, near the two cylinder walls, visible at $t=1.5$ sec. The meridional flow at this stage takes place along these isotherms, forming separate cells in the sidewall regions. The two cells are in the process of forming at this stage; some cross flow is evident, but this vanishes as the cells develop to the stage shown at $t=11.5$ sec. The cells can exist separately because the viscous effects induced by the container have not yet had enough time to transmit their influence to the interior regions of the fluid. As another consequence of this inviscidness, the meridional flow reaches its largest value, as is verified by stream function values and by the peak in the energy curve $E_k(\psi)$ of Fig. 15a, at about $t=8$ sec. The maximum conversion of potential energy to kinetic energy, $E_k:E_p$, at this instant also is associated with the maximum meridional flow.

The initial zonal velocity forms two bands of upper region westerlies, and lower region easterlies, with magnitudes reaching about 10 per cent of their final values. The maxima and minima are all located at the corners of fluid. The easterly maxima are roughly equal, with the slightly larger value occurring near the inner cylinder. The westerlies, on the other hand, have a pronounced maximum on the surface near the outer cylinder.

2. $t=11.5$ sec. As the flow progresses to $t=11.5$ sec, the 4 strong zonal velocity regions grow in size and reach 50 per cent of their final strengths. The individual nature of the two meridional cells causes the independent growth of these 4 regions. The region of maximum zonal velocity forms a jet whose core moves toward the inner cylinder as the flow evolves.

The isotherms display the effects of convection. Their lining up in the horizontal, near the base of the

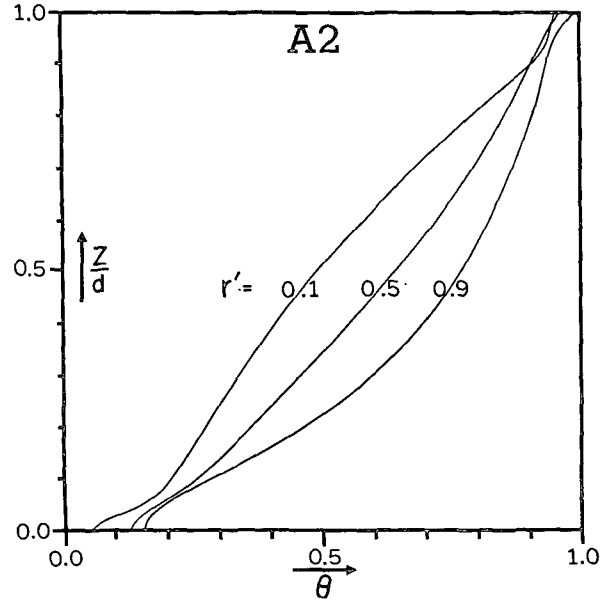

FIG. 13. The vertical distribution of normalized temperature at non-dimensional radii, $r'=0.1$, 0.5, and 0.9, for flow A2 with a fixed upper surface. Compare reduced spread of isotherms of A2 with those of A3 (Fig. 9).

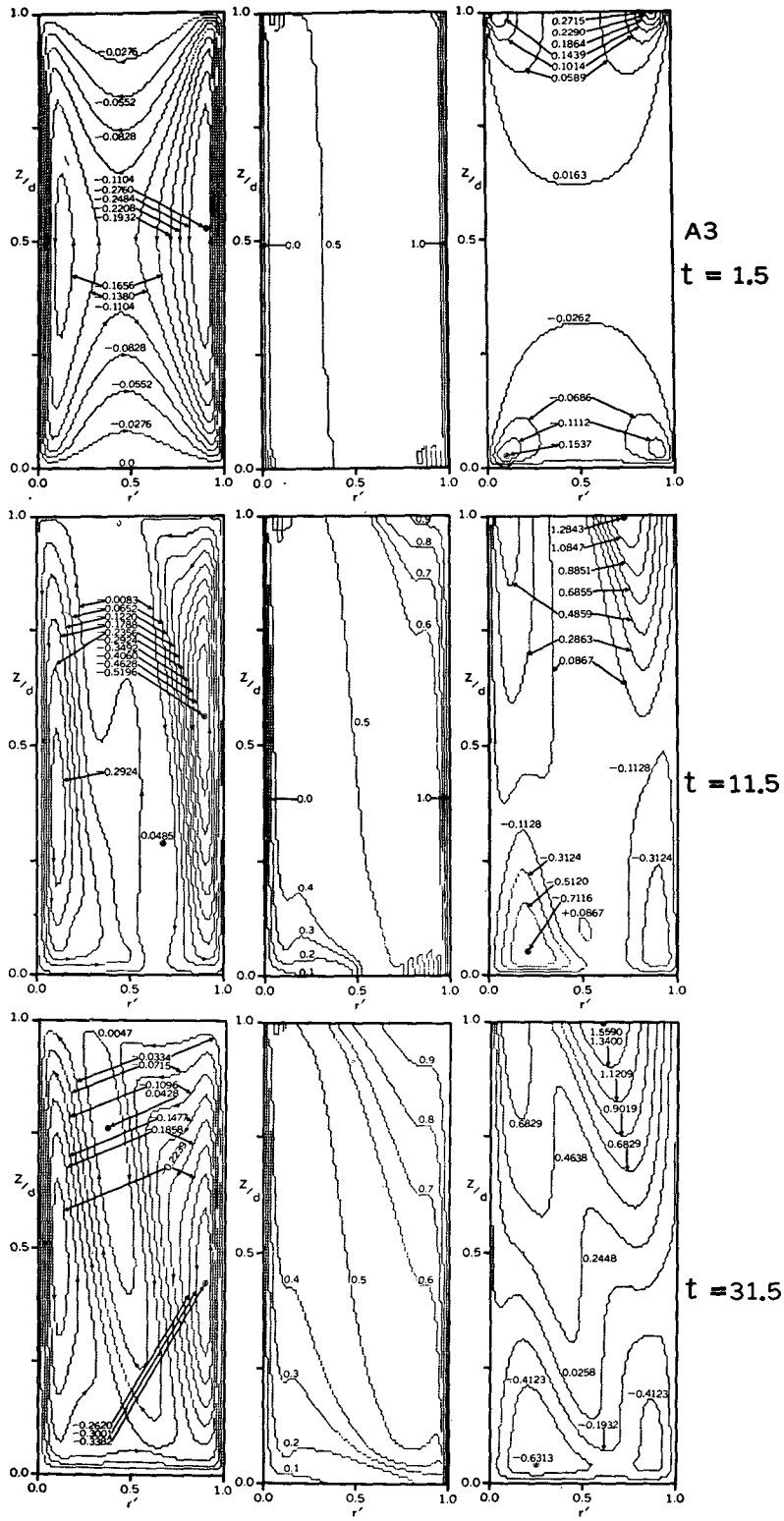

FIG. 14. The contours of stream function, temperature and zonal velocity at times of 1.5, 11.5, 31.5, 71.5, 111.5 and 151.5 sec illustrating the critical stages of the flow evolution of case A3. The steady state field at 286 sec is given in Fig. 2.

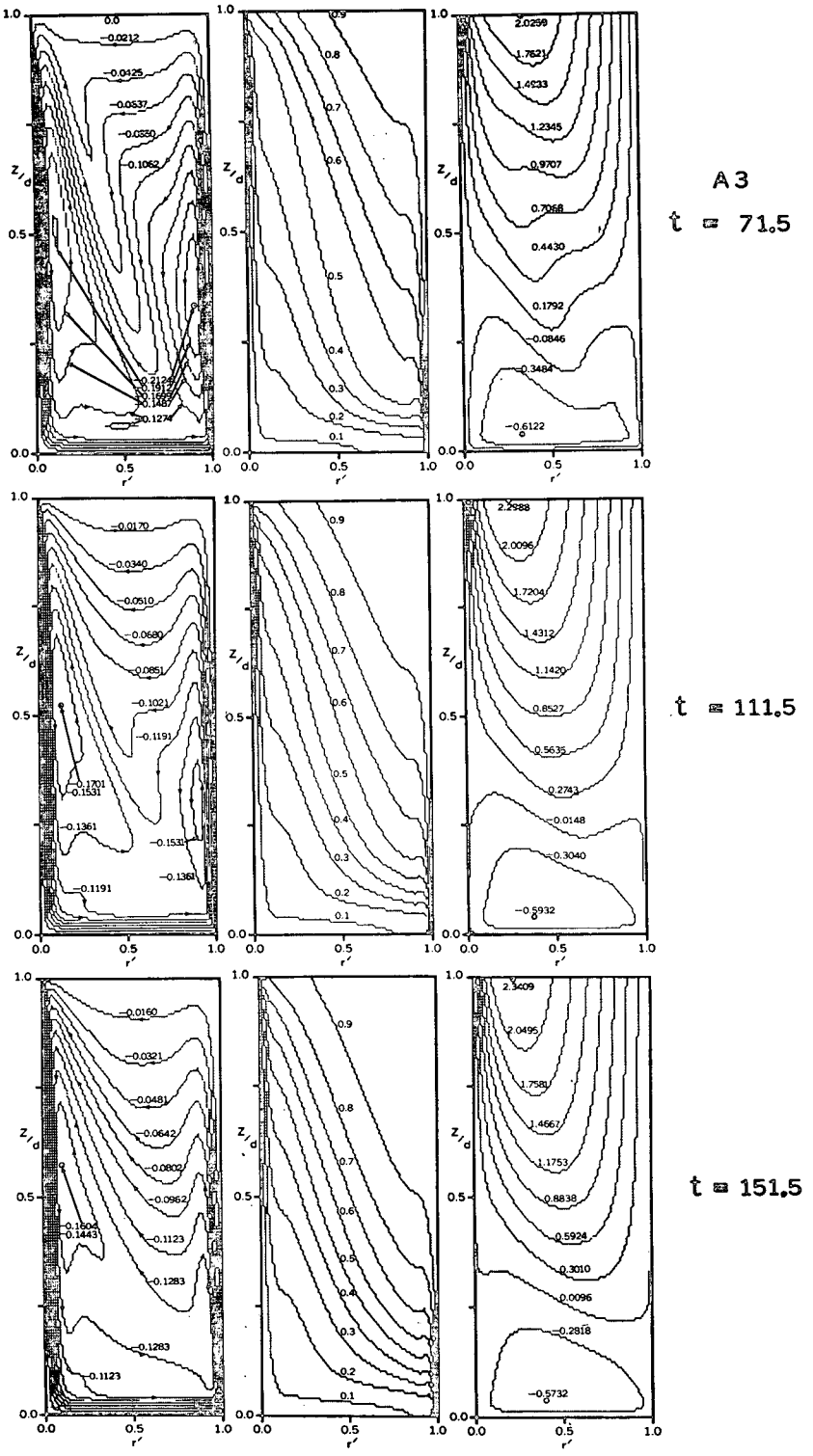

FIG. 14. (*Continued*).

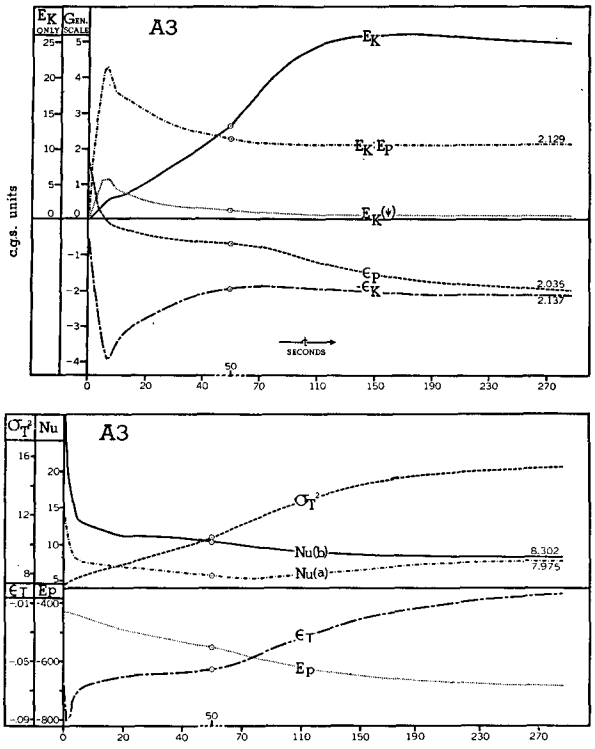

FIG. 15. a, b. The integral quantities as functions of time for flow A3. The time scale alters at 50 sec and is denoted by circles on the curves. The kinetic energy E_K has a separate scale. $E_K(\psi)$ is the meridional kinetic energy, E_K:E_P the potential to kinetic energy conversion, ϵ_K the kinetic energy dissipation, ϵ_T the temperature variance dissipation, ϵ_P the potential energy dissipation, E_P the potential energy, and σ_T^2 is the temperature variance. The Nusselt numbers Nu(a) and Nu(b) measure the heat transfer through the inner (cold) cylinder and outer (hot) cylinder.

inner cylinder and upper surface of the outer cylinder, is associated with the broadening of the meridional cells in those regions.

3. t=31.5 sec. The thermal boundary layers lead a separate existence for the first 31.5 sec, after which the isotherms of the cold wall layer merge into the hot wall layer, the latter being in the process of detaching itself from the upper part of the wall. The 0.5 isotherm acts as the dividing line between the two thermal boundary layers.

At 31.5 sec, an Ekman layer starts to form at the base and viscous forces become more active within the fluid. The viscously induced meridional flow spreads along the base and leads to a junction of the 2 cells. The meridional streamlines then take on the appearance of a tricellular system with the axis of the center cell coinciding with the 0.5 isotherm. The convection of the cold wall isotherms into the hot wall layer is associated with the joining of these cells.

The flow of the middle cell clearly parallels the isotherms, being, for example, downward along the 0.6 isotherm and upward along the 0.4 isotherm. The widening of the sidewall cells, at the upper surface for the hot wall and base for the cold wall, is associated with the joining of the base flow. The zonal flow, in joining up its jet-like regions, directly mirrors the meridional cell system. The maximum value of u continues to increase and approach the cold wall along the free surface.

4. t=71.5 sec. During the next 40 sec, the Ekman layer gathers strength, becoming fully formed at 71.5 sec. The isotherms continue to part from the walls and to slope linearly across the fluid, forming a fairly uniform pattern at this stage. The broadening of the sidewall boundary layers under the control of the isotherm field continues until the middle cell is more or less eliminated. The flow in the upper region no longer just dips down after rising up the hot wall, but penetrates along the free surface into the cold wall boundary layer. The zonal velocity undergoes a general smoothing out.

From Fig. 15 we notice that the kinetic energy has reached about 60 per cent of its final value and the energy conversion E_k:E_p has become more or less constant. The Nusselt number for heat extraction Nu(a) reaches the bottom of its decline at this stage.

From now on, the fluid changes occur under the slow acting diffusion processes. The strong shearing flow associated with opposing currents along the 0.5 isotherms at 71.5 sec cannot exist and decays through the action of friction forces. However, the Ekman layer on the base maintains the cell associated with the inner wall so that the resulting flow is one in which this cell dominates. The destruction of the central shear layer leads to the extinction of the hot wall cell, and results in a smooth upflow across the fluid interior.

The asymmetry of the flow is undoubtedly due to the free surface and its inability to form an Ekman layer. The hot wall flow then tends to separate from the outer cylinder and the Ekman layer at the base consequently supports a secondary cell of a size corresponding to the diminished boundary layer length. In the fixed surface experiments, the cells were consistently symmetric so that the absence of an Ekman layer on the upper surface leads to the asymmetric shape of the cell on the inner cylinder.

The final stage of the flow is essentially one of changes by conductive processes, there being a longer time scale for conductive processes than for frictional ones. Thus, whereas the kinetic processes (Fig. 15a) approach constant values near the 150-sec mark, the thermal processes continue to change for about 300 sec. A comparison of the contours at 151.5 sec (Fig. 14) and those at 286.5 sec, given in Fig. 2 (case A3), illustrates this distinction; for whereas the flow fields remain the same, the isotherms, particularly the 0.9 one, have continued to diffuse through the fluid.

The maximum zonal velocity at the jet core finally settles up at r'=1/4, having moved in from its initial starting point near r'=1.0.

4. Concluding remarks

A detailed representation of the structure of annulus convection can be constructed by numerical techniques. By experimenting with the finite difference resolution,

we have shown that the solutions obtained are accurate. In a subsequent paper, the accuracy of the numerical technique will be further verified by comparing directly with experimental observation. The boundary layers are incorporated explicitly into the scheme and together with the free flow are dealt with as a single system. Placing 3 grid points within each boundary layer provided ample representation of the layers as far as the total fluid system was concerned. The results confirm the practicality of obtaining numerical solutions for the more complex three-dimensional flows and of including their boundary layers explicitly.

Although the axisymmetric flow is not an atmospheric analogue, its solutions indicate what can be expected in those systems that are. The sidewall boundary layers form the most artifical element of the analogue. If the boundary layers play a passive rôle in other regimes, the annulus would better simulate the atmosphere. The boundary layers are most active in the angular momentum balance, forming a sink region at the inner cylinder and source on the base. The isotherms so arrange themselves that small source and sink regions of heat form in locations similar to those of the effective heat field of the atmosphere.

The application of Eady's criterion for geostrophic baroclinic instability decides one flow as being stable, the other unstable, in agreement with observation. The solutions also show the strong meridional flow across the isotherms that produces the energy transformation. Although Eady's model is barely valid for the annulus, it does indicate that baroclinic instability is the process leading to the wave regime.

Although the countercurrents associated with the sidewall boundary layers are weak, they do extend the influence of the boundary layers into the fluid interior. Robinson (1959) has explained the existence of such countercurrents for a conductively determined temperature field but it has not been determined whether his explanation can be extended to the convective type of flow. Whereas Robinson's theory associates the countercurrents with the rotational constraint of the Ekman layer, the transient contours indicate that the currents are associated with sidewall momentum layers but depend on the Ekman layer for their equilibrium existence.

In the transient flow the zonal jet forms on the outer cylinder and moves inward to its equilibrium point. This occurs despite the fact that in the steady state, the outer cylinder makes no contribution to the angular momentum balance. The zonal velocity is strongly coupled to the temperature field by the essentially geostrophic nature of the flow. However, the nonlinear term $(u^2/r)_z$ also makes a significant contribution to the vorticity balance. The complex balance of forces emphasizes the difficulty of forming an analytical theory for this problem.

The inhibiting effect of rotation upon heat transfer is clearly illustrated by the Ω^{-1} dependency of the Nusselt numbers for the two free surface flows. The Nusselt number also serves as an indicator of the attainment of a steady state, whereas the kinetic integrals reach steadiness before the final fields are formed.

Acknowledgments. The author wishes to express his appreciation of the interest and encouragement in this investigation shown to him by Dr. Kirk Bryan. He is further indebted to Miss M. B. Jackson for her assistance in preparing the graphical presentations of the numerical material. The author also wishes to acknowledge beneficial contacts with Mr. S. Piacsek of M.I.T. and Mr. C. Quon of Cambridge University who have performed similar studies.

REFERENCES

Barcilon, V., 1964: Rôle of the Ekman layers in the stability of the symmetric regime obtained in a rotating annulus. *J. Atmos. Sci.*, **21**, 291–299.

Bowden, M., and H. F. Eden, 1965: Thermal convection in a rotating fluid annulus: temperature, heat flow, and flow field observations in the upper symmetric regime. *J. Atmos. Sci.*, **22**, 185–195.

Eady, E. T., 1949: Long wave and cyclone waves. *Tellus*, **1**, 33–52.

Faller, A. J., 1958: Detailed measurements in Hadley regime symmetric convection. Final Report under contract AF19(504)-1292, University of Chicago, 5.1–5.8.

Fowlis, W. W., and R. Hide, 1965: Thermal convection in a rotating annulus of liquid: Effect of viscosity on the transition between axisymmetric and non-axisymmetric flow regimes. *J. Atmos. Sci.*, **22**, 541–558.

Fox, L., 1957: *The Numerical Solution of Two-Point Boundary Problems in Ordinary Differential Equations*. New York, Oxford University Press, 371 pp.

Fultz, D., R. R. Long, G. V. Owens, W. Bohan, R. Kaylor and J. Weil, 1959: Studies of thermal convection in a rotating cylinder with some implications for large-scale atmospheric motions. *Meteor. Monogr.*, Boston, Amer. Meteor. Soc., **4**, No. 21, 1–104.

Hide, R., 1958: An experimental study of thermal convection in a rotating fluid. *Phil. Trans. Roy. Soc.*, London, **A250**, 441–478.

Lighthill, M. J., 1963: *Laminar Boundary Layers*. London, Oxford University Press, 46–60.

Lilly, D. K., 1964: Numerical solutions for the shape-preserving two dimensional thermal convection element. *J. Atmos. Sci.*, **21**, 83–98.

Lorenz, E. N., 1962: Simplified dynamic equations applied to the rotating-basin experiments. *J. Atmos. Sci.*, **19**, 39–51.

Pearson, C. E., 1965: A computational method for viscous flow problems. *J. Fluid Mech.*, **21**, 611–622.

Phillips, N. A., 1959: An example of non-linear computational instability. *The Atmosphere and the Sea in Motion*, New York, Rockefeller Institute Press and London, Oxford University Press, 501–504.

Richardson, L. F., 1922: *Weather Prediction by Numerical Process*. London, Cambridge University Press, 236 pp.

Richtmyer, R. D., 1957: *Difference Methods for Initial-Value Problems*. New York, Interscience, 101–104.

Robinson, A. R., 1959: The symmetric state of a rotating fluid differentially heated in the horizontal. *J. Fluid Mech.*, **6**, 599–620.

Smagorinsky, J., 1963: General circulation experiments with the primitive equations: I. The basic experiment. *Mon. Wea. Rev.*, **91**, 99–164.

Veronis, G., 1966: Wind driven ocean circulation—Part 2. Numerical solutions of the non-linear problem. *Deep-Sea Research*, **13**, 31–55.